

Interpretation of the harmonic response of superconducting films to inhomogeneous ac magnetic fields

G. D. Poulin, J. S. Preston, and T. Strach

Department of Engineering Physics, McMaster University, Hamilton, Ontario, Canada L8S 4M1

(Received 28 December 1992; revised manuscript received 16 March 1993)

We present a quantitative analysis of the response of a thin superconducting film to an applied nonuniform ac magnetic field. The analysis is directly applicable to the single-coil inductive measurement technique where a small coil driven by an ac current produces a nonuniform field, with J_c determined by the appearance of a third-harmonic component of the voltage generated across the coil. We derive a simple model to explain the response of the film to the applied magnetic field in the absence of weak links. This model is used to predict the third-harmonic voltage generated across the coil. The derivation of the model explains why superconducting films having thicknesses even less than the penetration depth screen out the nonuniform ac magnetic fields generated by the coil. A simplified version of the model yields analytic expressions that describe the magnitude and phase of the third-harmonic component at high drive currents while the full model yields excellent agreement with experimental measurements for our highest quality epitaxial films. In other films, the presence of weak links leads to a characteristic signature in the harmonic response at low drive currents. We have also found that ion irradiation can reduce the critical current densities by significant amounts without introducing weak links into the film.

I. INTRODUCTION

In 1987, high-quality epitaxial film growth of oxide superconductors was demonstrated.¹ It was immediately clear that a nondestructive method for evaluating film quality was required. One class of techniques, capable of measuring both the critical temperature (T_c) and the critical current density (J_c) of superconductors, employs a small inductive coil placed in proximity to a superconducting film. The coil is driven at a low frequency by an ac source, producing an inhomogeneous magnetic field. Information regarding the film is derived by measuring the response of the film to the applied field. When the magnitude of the applied field is increased beyond a critical level, dissipation is observed in the film. Initially, experiments were performed using two coils, with one as the drive coil, and the second as the pickup coil.²⁻⁴ This technique requires accurate alignment of the two coils, and, when the coils are placed on opposite sides of the film, makes it difficult to establish good thermal contact to the film. Claassen, Reeves, and Soulen⁵ pioneered the use of a single coil, where this coil is used as both the drive coil and the pickup coil. They described a technique to measure both T_c and J_c of a superconducting film with their apparatus. For the latter, they used the method of images to determine the lateral current distribution induced in the film for a given coil drive current provided that the current density in the film remained below J_c and that the film was thick enough for the assumption of complete screening to be valid. This provided a calibration factor, so that the onset of nonlinearity in the film response could be identified with the critical current density of the film. The onset of the nonlinearity was sensitively detected by the appearance of a third-harmonic component in the voltage generated across the coil.

Critical current densities have also been determined from ac susceptibility measurements as a function of field intensity both directly⁶ and through the onset of odd harmonics.⁷ The microcoil experiments have two principle advantages over this technique. First, a simple, accurate calibration of the induced current density versus applied field is more difficult in an ac susceptibility geometry. However, we note that the detailed numerical model presented in this paper could be simply modified to calculate the lateral current distributions for circular films in an ac susceptibility geometry. The second and more important advantage of the microcoil experiments is that the current distributions are confined under the coil. As a result, the technique is not sensitive to reductions in J_c at the edges of the film or to variations in the shape of the sample.

In this paper, we will investigate the film response to nonuniform ac magnetic fields, such as those produced by the single coil in the inductive measurements described above. We first develop a simple argument based on Faraday's law and the first London equation, which accounts for the effective screening of small magnetic fields applied by the drive coil even by films thinner than the magnetic penetration depth. This argument can be extended to describe the currents induced in the film without the assumption of perfect screening. The resulting model is then applied to determine the lateral distribution and the wave form of the induced currents even if the critical current density is reached during part of the ac cycle. From a Fourier analysis of this result, we obtain the magnitude and phase of the third-harmonic signal for all drive currents. A simplified version of this model yields a convenient analytical expression which agrees with experimental data for moderate to large drive currents. A complete numerical solution of the model gives excellent agreement at all drive currents for very

high-quality films. Measurements carried out on epitaxial films of slightly lower quality have harmonic components in excess of the prediction from the model at low drive currents. We attribute this to the presence of weak links within the film, resulting in a range of critical currents.

II. APPARATUS

The coil and a Lakeshore Cryotronics DT-470-SD-12A diode were mounted in a Teflon cylinder. The sample was held with the film in contact with both the coil and the diode by a spring-loaded copper block. T_c and J_c were determined by measuring the voltage generated across the coil as a function of temperature and drive current, respectively.

The apparatus can be used to determine the critical temperature of a superconducting film by measuring the change in the net inductance of the coil-film pair when the film goes through the superconducting transition. For these measurements, a low amplitude 1-mV drive voltage was used, typically inducing a film current density of 10^4 A/cm². This value was small enough so that the transition width was independent of the drive voltage. The magnitude and phase of the voltage across the coil were measured using a Stanford Research SR530 dual channel lock-in amplifier. The voltage across the coil is given by

$$V_0 e^{j\phi_0} = V_i e^{j\phi_i} \left[\frac{j\omega L + R_L}{j\omega L + R_L + R_0} \right], \quad (1)$$

where R_L and L refer to the resistance and inductance of the coil, and R_0 is the output impedance of the source. Solving Eq. (1) for the coil inductance L is straightforward, since the magnitude and phase of the applied voltage are known, and the magnitude and phase of the output voltage are measured. A typical relation between inductance and temperature is shown in Fig. 1.

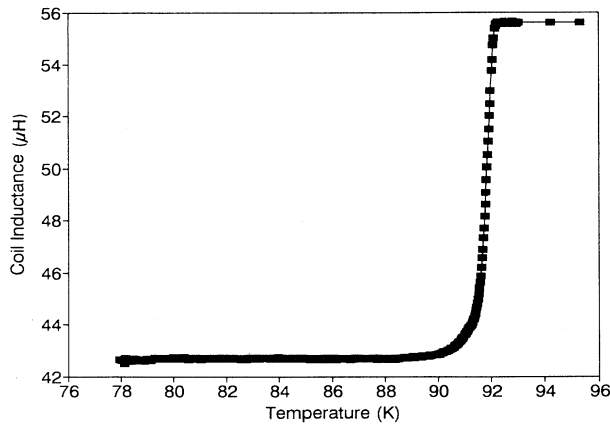


FIG. 1. Graph showing measured coil inductance vs temperature for a $Y_1Ba_2Cu_3O_7$ film. There is a rise in the inductance as the film is warmed through T_c .

Critical current density measurements

The critical current density was measured using the apparatus shown in Fig. 2. A second channel of the digital voltmeter (DVM) was connected across a 1-Ω reference resistor in series with the coil to allow measurement of the coil current magnitude. In order to detect the third-harmonic component, the multifunction synthesizer was configured to supply the drive current at ω_0 , and a reference signal at $3\omega_0$ for the lock-in amplifier. To avoid saturating the lock-in amplifier with the large amplitude fundamental component, a third-order high-pass filter was inserted between the coil and the amplifier input.

The critical current density measurements were carried out at 30 kHz. This frequency maximized the signal-to-noise ratio for our apparatus. In Sec. III, it will be shown that the third-harmonic signal is proportional to the drive frequency. The dominant noise source at $3\omega_0$ in our experiments was found to be the voltage produced by the multifunction synthesizer. This was determined to be independent of frequency. However, for a given output noise voltage V_n the voltage appearing at the lock-in amplifier is

$$V_0 = \left[\frac{R_L + R_1 + j\omega L}{R_0 + R_L + R_1 + j\omega L} \right] V_n, \quad (2)$$

where R_1 is the 1-Ω reference resistor. Since V_n is independent of frequency, the measured noise level increases sublinearly with frequency and the signal-to-noise ratio improves. In our apparatus, the maximum frequency was limited by the lock-in amplifier.

Measurements of third-harmonic magnitude and phase are shown as a function of drive current in Fig. 3. Following Claassen, Reeves, and Soulen,⁵ a calibration between film current density and coil drive current has been carried out, as shown at the top of the graph. It is

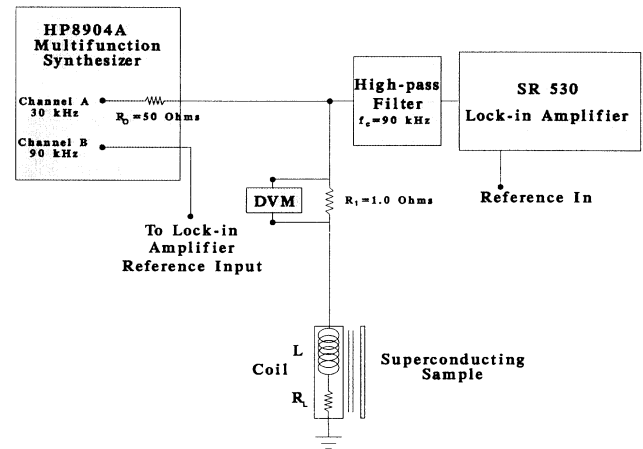


FIG. 2. Apparatus used to measure critical current densities. Channel A is driven at 30 kHz, while channel B, used as the reference input to the lock-in amplifier, is driven at 90 kHz. The digital voltmeter (DVM) is used to measure the coil current.

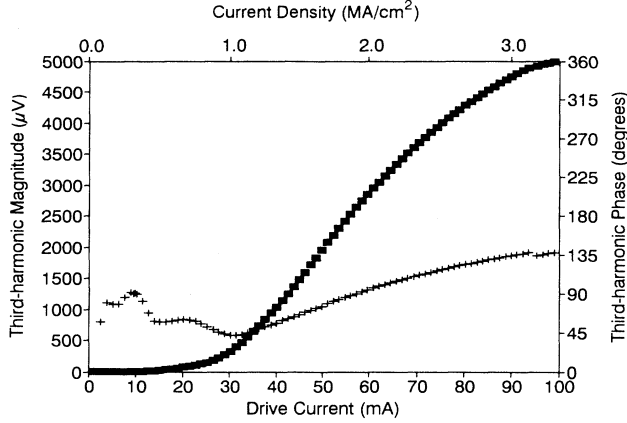


FIG. 3. Typical J_c measurement curve for a $Y_1Ba_2Cu_3O_7$ film at 77 K. The third-harmonic magnitude and phase are shown as a function of drive current. The technique of Claassen, Reeves, and Soulen (Ref. 5) has been used to convert drive current to film current density.

difficult to determine the onset of the third-harmonic component and hence J_c from this graph. A linear extrapolation of the curve gives a J_c of 1 MA/cm². In Sec. III, a model for the magnitude and phase of the third-harmonic versus drive current will be developed providing a method for using the entire curve to determine J_c .

Two different coils were used for the films characterized in this paper. A 426-turn coil was used for the measurements in Figs. 3 and 8, while a 234-turn coil was used in Figs. 5 and 7. Different drive-current to current-density calibrations were therefore necessary; the actual calibrations are shown in each figure. Additionally, due to the different coil geometries, measured third-harmonic magnitudes in Fig. 3 and 8 are not directly comparable with those in Figs. 5 and 7. All J_c measurements were carried out at 77 K.

III. SINGLE ANNULUS MODEL

In this section, a simplified model identifying the origin of the harmonic response of epitaxial films to the applied ac magnetic fields produced by large coil drive currents will be developed. In this context, large drive currents induce critical current densities in the film. We will also show that the film is very efficient at screening out small applied magnetic fields. A requirement for calibrating the film current density to the coil drive current⁵ is that the applied field be perfectly shielded from the back surface of the film. We will show that even for films considerably thinner than the magnetic penetration depth λ , perfect screening is an excellent approximation. Kittel, Fahey, and Louie⁸ have considered the related problem of a cylinder with a superconducting surface layer in a uniform ac magnetic field applied parallel to the film. Applying the first London equation and Faraday's law, they showed that the field inside the cylinder is reduced by a factor λ^2/Dt , where D is the diameter of the cylinder, and t is the thickness of the superconducting surface layer. We will use a similar approach to analyze the prob-

lem of interest here: a planar film with an ac field applied perpendicular to the film.

In the derivation below, we assume that the induced current is uniform throughout the thickness of the film and between the radii r_{inner} and r_{outer} . This current distribution defines an annulus having an average radius $r = (r_{inner} + r_{outer})/2$, a width $w = (r_{outer} - r_{inner})$, and a thickness t . Using either the technique of Claassen, Reeves, and Soulen⁵ or our method developed in Sec. IV, the film current density is found to extend only slightly beyond the edge of the coil (see Fig. 6 with a drive current of 30 mA or less) and we identify the radius and width of the annulus with the radius and width of the coil.⁹

Let the coil drive current be $\text{Im}[I_D e^{j\omega t}]$, as shown in Fig. 4(a). The electromotive force (\mathcal{E}) induced in the annulus will be

$$\mathcal{E}_{ann} = -\frac{d\Phi_{ann}}{dt} = -\frac{d}{dt}[MI_D + LI_{ann}], \quad (3)$$

where Φ_{ann} is the net flux in the annulus, M is the

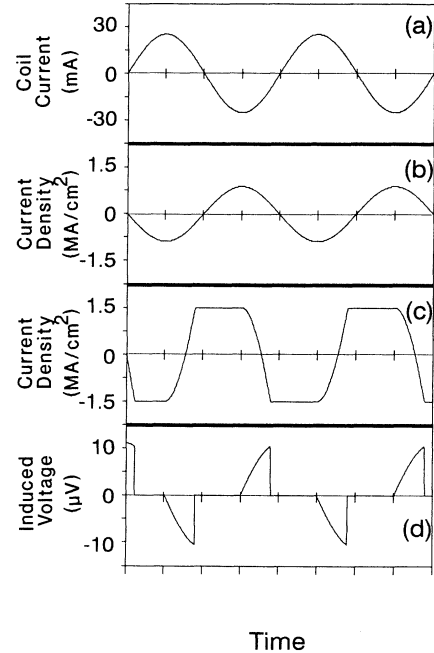


FIG. 4. These figures represent idealized data used to derive the third-harmonic response based on the single annulus model. (a) shows the current in the drive coil as a function of time. (b) shows the current density induced in the annulus for small drive currents if J_c is not reached during the drive current cycle. Note that the current density is 180° out of phase with the drive current. (c) shows the current density induced in the annulus for large drive currents. Once J_c is reached the film current density saturates but becomes unsaturated as soon as the drive current magnitude begins to decrease. As a result, the curve crosses zero at a different time than the trace in (b). (d) shows the \mathcal{E} induced in the drive coil due to the current density shown in (c). The third-harmonic content of this wave form is derived using Fourier analysis.

coefficient of mutual inductance between the coil and the annulus, L is the self-inductance of the annulus, and I_{ann} is the current induced in the annulus. Assuming sinusoidal steady state,

$$-j\omega MI_D e^{j\omega t} - j\omega LI_{\text{ann}} e^{j\omega t} = I_{\text{ann}} e^{j\omega t} Z_{\text{ann}}, \quad (4)$$

where Z_{ann} is the impedance of the annulus. Using the first London equation, the impedance of the annulus is given by

$$Z_{\text{ann}} = \frac{l}{\sigma A} = \frac{2\pi r j \omega \mu_0 \lambda^2}{wt}, \quad (5)$$

where l is the length of the annulus, σ is its conductivity, and A is its cross-sectional area. Note that we have approximated the conductivity of the superconductor by the imaginary component only, and have ignored the real component due to normal-state electrons. Very close to T_c or at high frequencies, the real component would have to be included.

Solving for the annulus current in terms of the drive current gives

$$I_{\text{ann}} = - \left[\frac{M}{L + (2\pi r/tw)\mu_0\lambda^2} \right] I_D. \quad (6)$$

From Eq. (6), we see that the annulus current will be 180° out of phase with the drive current as shown in Fig. 4(b).

The net flux that links the annulus will be

$$\Phi_{\text{ann}} = MI_D + LI_{\text{ann}} = MI_D \left[\frac{\mu_0\lambda^2 2\pi r/tw}{L + \mu_0\lambda^2 2\pi r/tw} \right]. \quad (7)$$

Simplifying this expression gives us

$$\Phi_{\text{ann}} = MI_D \left[\frac{l}{t+l} \right], \quad \text{where } l = \frac{2\pi r \mu_0 \lambda^2}{Lw}. \quad (8)$$

If the film was not present, the net flux would be MI_D . Provided that the film is much thicker than l , then the presence of the film will result in a decrease in the net flux by a factor l/t . An approximate expression for the self-inductance of an isolated current loop is given in Van Duzer¹⁰ as

$$L = r\mu_0 \ln \left[\frac{16r}{w} - 2 \right]. \quad (9)$$

Substituting this into (7) gives us the condition on film thickness for significant flux reduction:

$$t \gg l \simeq \frac{2\pi\lambda^2}{w \ln(16r/w - 2)}. \quad (10)$$

For our coils, the annulus width w is determined by the width of the coil. As noted in Ref. 9, if the coil is extremely narrow, then the annular width is determined instead by the coil to film separation.

Assuming that the radius and width of the annulus are approximately 1 mm and that the penetration depth is 0.2 μm , Eq. (10) becomes $t \gg 0.05$ nm. Of course, Eq. (10) is not expected to hold down to submonolayer film thicknesses, however, it demonstrates the ability of thin

films to effectively screen inhomogeneous fields produced by small coils. For our geometry, with a film thickness of 250 nm, a radius of 2 mm, and an annular width of 0.5 mm, the presence of the film will reduce the flux to 5×10^{-4} of its original value. We note that our analysis is based on kinetic arguments only; it is only valid for ac applied fields and is independent of the Meissner effect. It also requires that the applied field does not extend beyond the edge of the film and hence is inappropriate for ac susceptibility geometries. Of course, it is only valid for drive currents small enough so that the induced current density in the film is everywhere below J_c .

Claassen, Reeves, and Soulen argued⁵ that the expression for the field screening from Ref. 8, λ^2/Dt , could be used in a planar geometry with D interpreted as the diameter of the coil so that even thin superconducting films would provide excellent shielding for inhomogeneous fields. Our analysis [Eq. (10)] demonstrates that this argument is essentially correct, with the diameter replaced by the width of the coil.

We now derive the induced current wave form for large drive currents and extract from it the harmonic response. Once the critical current density is attained, image currents cannot be used to compute the current density in the film. The response of a superconductor to an induced electromotive force which drives the current density to its critical value has been described by Ishida and Mazaki.¹¹ Essentially, the superconductor acts as an ideal inductor and sustains the magnetic flux while the current density is less than J_c . Figure 4(c) shows what occurs when the drive current is large enough to induce critical current densities in the film. When the current density reaches the critical current density of 1.5 MA/cm², it saturates, and flux begins to enter the film. Flux will continue to enter the film until the derivative of the applied field changes sign. At this point, the magnitude of the induced current decreases, preserving the flux at a constant value. This continues until the current density again exceeds J_c (with opposite polarity), then the cycle repeats itself.

The \mathcal{E} induced in the drive coil can be calculated using the annulus current density as a function of time as shown in Fig. 4(c). It is given by

$$\mathcal{E}_{\text{coil}} = - \frac{d\Phi_{\text{coil}}}{dt} = -M \frac{dI_{\text{ann}}}{dt} - L_{\text{coil}} \frac{dI_D}{dt}, \quad (11)$$

where L_{coil} is the self-inductance of the coil. Since the only nonsinusoidal contribution is from the film current, only the first term above will have harmonic content. Shown in Fig. 4(d) is the contribution to the coil \mathcal{E} due to the mutual coupling to the film. Note that, since the wave form has half-wave symmetry, only odd harmonics will exist. Carrying out Fourier analysis on the wave form in Fig. 4(d) allows us to calculate the third-harmonic content. This has been done analytically as a function of drive current and critical current density. The third-harmonic magnitude based on this model is predicted to be

$$V_{3f} = \frac{8M\omega_0 I_c}{2\pi} \left[1 - \frac{I_c}{I_D} \right], \quad (12)$$

where ω_0 is the drive frequency, and I_c is the coil critical current, i.e., the current in the drive coil when the induced film current density reaches J_c . Note that the third-harmonic component will be zero if the drive current is less than I_c ; Eq. (12) is valid only for drive currents which exceed I_c . The phase of the third-harmonic is similarly given by

$$\Phi_{3f} = -\tan^{-1} \left[\frac{4(I_D/I_c - 1)^{1/2}(I_D/I_c - 2)}{(I_D/I_c)^2 - 8(I_D/I_c) + 8} \right]. \quad (13)$$

We note that Eqs. (12) and (13) predict that there are universal curves for both the magnitude and phase of the third-harmonic. Equation (12) predicts that the third-harmonic magnitude saturates at a value proportional to J_c . Films with larger critical current densities will give larger third-harmonic signals.

Shown in Figs. 5(a) and 5(b) are third-harmonic measurements made on a high-quality film before and after ion-beam irradiation. Prior to irradiation, this film had a 1-K superconducting transition width. After the second irradiation dose, T_c dropped by 5.5 K, and the width broadened to 4 K. Optical conductivity measurements made on this film will be presented elsewhere,¹² however we note that the results indicate that the scattering rate of the carriers has been increased, while the carrier density remained constant. This film was used to investigate the dependence of the third-harmonic response to changes in J_c , since the film geometry and thickness is then constant for all measurements.

Figure 5(a) shows measured third-harmonic magnitude data along with a theoretical prediction using Eq. (12). In all cases, the fit gives good agreement to the data for large drive currents, although it deviates in the region where the third-harmonic onset occurs. This discrepancy is due to approximating the current distribution as uniform across a single annulus. In Sec. IV, the calculation will be extended by approximating the film as being made up of multiple concentric annuli and including the coupling between the annuli. In Fig. 5, only the comparison of the single annulus model with the magnitude of the third-harmonic signal is shown. The calculated phase shows similar agreement with the data; good agreement is obtained for currents well above the critical value.

Equation (12) also predicts that the third-harmonic magnitude plotted against $1/I_D$ will yield a straight line having an x intercept at $1/I_D = 1/I_c$. Figure 5(b) shows the third-harmonic magnitude data plotted versus $1/I_D$. The extrapolated x intercept therefore provides a quick way to estimate J_c without having to measure the third-harmonic over a large range of drive currents. The curves in Fig. 5(b) all show linear behavior for large drive currents. We have found that to extrapolate the data and obtain an accurate value for the intercept requires currents corresponding to a minimum of four times the critical current. This criterion is satisfied for two of the three measurements shown in Fig. 5(b). It is not satisfied for the unirradiated sample, resulting in difficulties in accurate extrapolation. More data at large drive currents are necessary for this sample for estimation of the extrapolated x intercept.

An advantage of plotting the data in this way is that only two or three points at small $1/I_D$ are necessary for a rapid estimate of the critical current provided they are taken at sufficiently high drive currents. We have noted that the single annulus model overestimates J_c . By comparing the single annulus results with the more elaborate numerical calculation described in Sec. IV, we have determined that the overestimate is consistently a factor of 1.8. This factor can be confirmed by examination of the comparisons in Fig. 5(b). The x intercept of the extrapolation predicts that J_c is reached at a drive current of 15.7 mA for the 1×10^{14} He⁺/cm² data. From Fig. 5(a), it is clear that J_c is actually reached at a drive current of 8.7 mA. Note that this factor of 1.8 is independent of the experimental configuration. It is valid

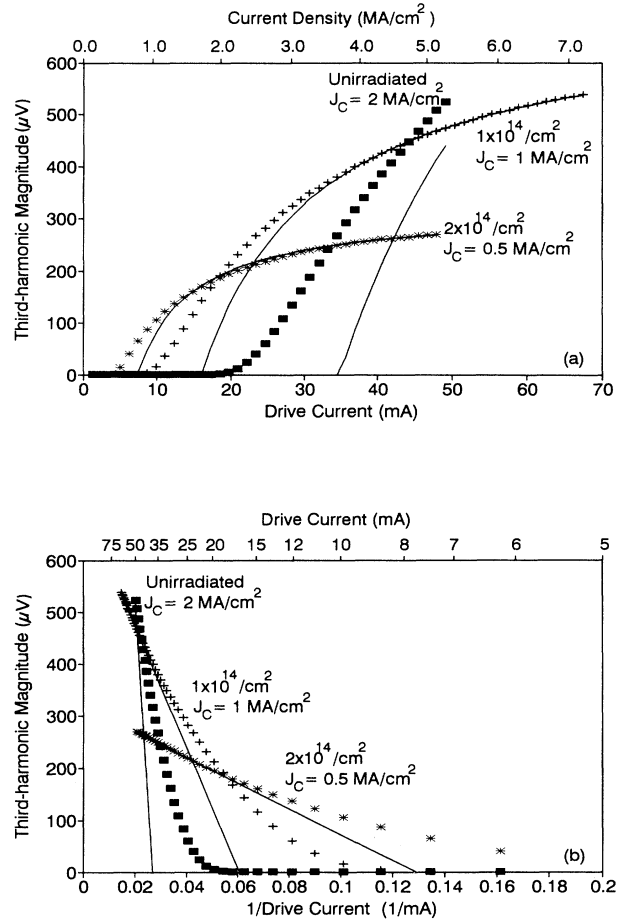


FIG. 5. (a) shows experimental (data points) and modeled (solid lines) data for a $Y_1Ba_2Cu_3O_7$ film after 160-keV He⁺ irradiation, measured at 77 K. The single annulus model has been used for the fit. Note that J_c decreases with increasing ion dose. The model fits the data well at large drive currents, but there is deviation at small drive currents. For the unirradiated sample, the model is beginning to approach the experimental data, but more data at large drive currents are needed for the model to agree with the data. (b) shows the data of (a) plotted vs $1/(\text{drive current})$.

for all the data presented here, and can also be used with data presented in Ref. 5.

IV. MULTIPLE ANNULUS MODEL

In this section the film will be modeled as a number of concentric annuli. Each annulus is constrained by the same critical current relationship described above in the single annulus case, however, there is mutual coupling between each of the annuli as well as between each annulus and the drive coil.

If the film is divided into N concentric annuli, the \mathcal{E} induced in the i th annulus will be

$$\begin{bmatrix} M_{1,1} + \mu_0 \lambda^2 \frac{2\pi r_1}{w_1 t} & M_{1,2} & \cdots & M_{1,N} \\ M_{2,1} & M_{2,2} + \mu_0 \lambda^2 \frac{2\pi r_2}{w_2 t} & \cdots & M_{2,N} \\ \vdots & \vdots & \vdots & \vdots \\ M_{N,1} & M_{N,2} & \cdots & M_{N,N} + \mu_0 \lambda^2 \frac{2\pi r_N}{w_N t} \end{bmatrix} \begin{bmatrix} I_1 \\ I_2 \\ \vdots \\ I_N \end{bmatrix} = - \begin{bmatrix} M_{D,1} I_D \\ M_{D,2} I_D \\ \vdots \\ M_{D,N} I_D \end{bmatrix}, \quad (15)$$

where the impedance of each annulus has been expanded as in Eq. (5). Inverting this matrix allows us to solve for the magnitude of the current in each annulus. Note that all annulus currents will be 180° out of phase with the drive current. The coefficients of self- and mutual inductance were obtained by interpolating from tables.¹³ The algorithm proceeds by computing the actual value of each annulus current at time t . Once the current in any annulus reaches the critical current density, it saturates and that annulus no longer contributes to the \mathcal{E} . For the purpose of calculating the current in the other annuli, the saturated annulus is removed from the system and the current magnitudes are recalculated for the $(N-1)$ annulus system. As the drive current continues to increase, other annuli may saturate and the order of the matrix is further reduced. When the drive current reaches its maximum value and begins to decrease, all terms in the matrix must be reincluded. At each point in the calculation where the order of the matrix is changed, the initial conditions are set by the requirement that each annulus current must remain continuous. At each time t , the \mathcal{E} induced in the coil is calculated from

$$\mathcal{E}_{\text{coil}} = - \left[L \frac{dI_D}{dt} + \sum_{p=1}^N M_{D,p} \frac{dI_p}{dt} \right], \quad (16)$$

where again, the summation is over all the annuli. When a current exceeds the critical current density, it saturates, and no longer contributes to the \mathcal{E} in the coil. Annulus currents and coil \mathcal{E} 's are calculated over a complete cycle of the drive current, and the third-harmonic content is computed using Fourier analysis.

Shown in Fig. 6 is a graph depicting the model peak annulus current density as a function of distance from the

$$\mathcal{E}_i = - \frac{d\Phi_i}{dt} = - \left[M_{D,i} \frac{dI_D}{dt} + \sum_{p=1}^N M_{i,p} \frac{dI_p}{dt} \right] = I_i Z_i, \quad (14)$$

where $M_{i,p}$ is the coefficient of mutual inductance between the i th and p th annulus, $M_{D,i}$ is the mutual inductance between the drive coil and the i th annulus, I_p is the current in the p th annulus, and the summation is over all the annuli. For convenience, $M_{i,i}$ is the self-inductance of the i th annulus. Expanding this expression for N annuli, an $N \times N$ matrix results, as shown below:

center of the film for various drive currents. The position of the coil relative to the film is shown schematically at the top of the figure. Until a drive current of 40 mA, J_c has not been reached in the film, and the peak amplitude scales linearly with the drive current. The shape of the curves below the critical current density is very similar to the current distribution calculated by Claassen, Reeves, and Soulen⁵ using a method of images. This is consistent with the results of Sec. III, where it was shown that less than 0.1% of the applied flux penetrates the film for small

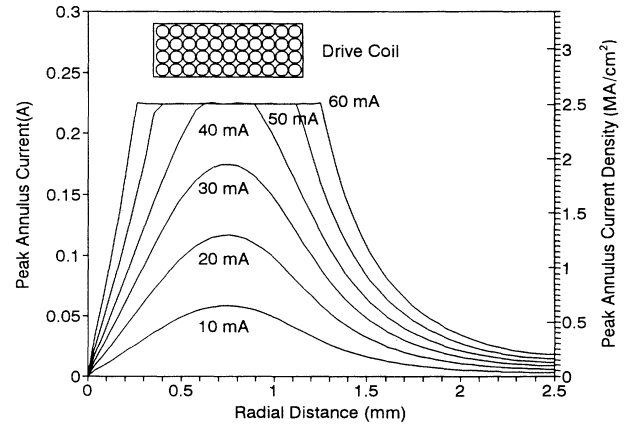


FIG. 6. Peak annulus current as a function of radial distance for various coil drive currents, as modeled by the multiple annulus model. The position of the drive coil is shown schematically above the curves. For clarity, only half of the coil and film are shown.

drive currents. The multiple annulus model can estimate the current distribution after J_c is reached, when the image current method breaks down. In this example, the critical current density has been reached when the drive current reaches 40 mA. For drive currents above 40 mA, the model predicts that the current distribution will saturate at the critical current density and broaden as intuitively expected.

The predicted third-harmonic magnitude and phase can also be extracted from the multiple annulus model. As seen in Sec. III, the single annulus model predicts that both the magnitude and phase of the third-harmonic signal will fall on a universal curve. The magnitude data are normalized by plotting V_{3f}/I_c against I_D/I_c . The phase data are normalized by plotting the third-harmonic phase versus I_D/I_c . This universality is retained in the multiple annulus model. Shown in Fig. 7(a) and Fig. 7(b) are normalized magnitude and phase data, respectively, for the

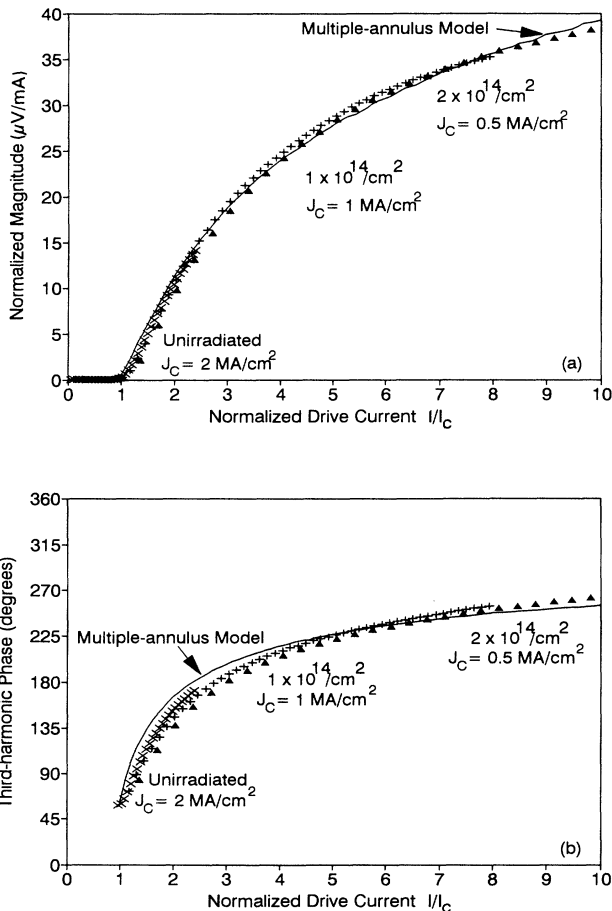


FIG. 7. (a) shows third-harmonic magnitude data of Fig. 5(a) after normalization. Predicted results based on the multiple annulus model are shown by the solid line. Note that the multiple annulus model gives good agreement to the data over all drive currents, and all the data fall on the same universal curve. (b) shows third-harmonic phase data after normalization. The solid line shows predicted results based on the multiple annulus model.

data shown in Fig. 5(a). The solid line shows the prediction based on the multiple annulus model. The data all lie on a universal curve. Additionally, while the single annulus model consistently overestimates J_c , the multiple annulus model gives excellent agreement both in the vicinity of J_c , and at large drive currents.

The agreement between the model and the measured response in Fig. 7 indicates that the critical current in the film can be modeled with a single parameter. It is remarkable that this continues to be the case even after irradiation has reduced J_c by a factor of 4. We defer to a later publication the detailed discussion of the optical and transport properties of these irradiated films, however, we note that a two-fluid interpretation of the optical conductivity indicates that the superfluid fraction has been strongly suppressed by the irradiation. The analysis of the microcoil data indicates that this has been achieved while retaining uniformity throughout the film.

The measurements described above can be contrasted with the measurements shown in Fig. 3 for a slightly lower quality epitaxial film, as inferred from critical current measurements and our harmonic analysis. In Fig. 8, the deviation of these measurements from a fit to the model are shown. As can be seen in the inset, the model describes the harmonic response accurately at large drive currents. We attribute the discrepancy at low drive currents to a local reduction in the critical current density due to weak links in this sample.

In a sample with weak links at sufficiently low drive currents, the current distribution in the film will be annular to provide the maximum shielding. At moderate drive currents, the shielding currents in the film will avoid the weak-link region. Therefore, during a cycle of

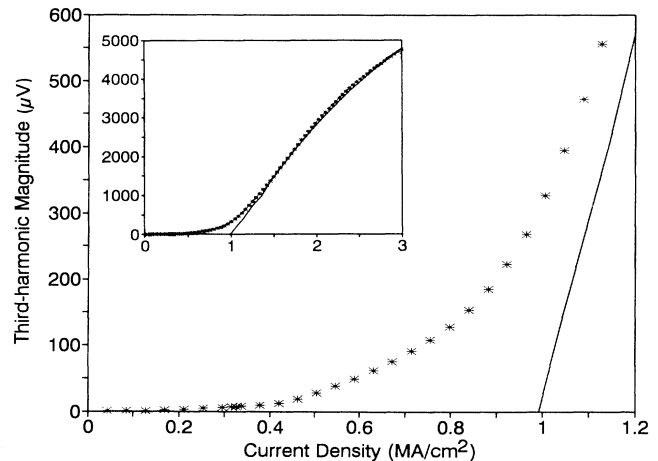


FIG. 8. The data from Fig. 3 and a fit (solid line) using the multiple annulus model. The graph shows the third-harmonic magnitude for small drive currents, where there is poor agreement between experimental and predicted signals. The inset shows data to larger drive currents, where the agreement is much better. The poor agreement at low drive currents suggests the presence of weak links which locally reduce the critical current density.

the ac drive current, the path of the shielding currents through the film will vary, leading to a harmonic response in the drive coil. At larger drive currents the critical current in the bulk of the film will be attained and the harmonic response will be described by our model. A single inductive measurement can provide an indication of the presence of weak links in addition to determining the critical current density in the bulk of the film. Many transport measurements would have to be carried out on different patterned bridges to provide the same information, since in that case, a bridge either would or would not contain a weak link.

We note that the presence of isolated weak links cannot be readily inferred from standard characterization techniques. For example, the film in Figs. 3 and 8, which has many weak links present, has $T_c = 91$ K, $\Delta T_c = 1$ K, and $J_c = 1$ MA/cm² at 77 K. The irradiated film of Figs. 5 and 7 has T_c 's of 91.5, 90, and 86 K, ΔT_c 's of 1, 2.5, and 4 K, and J_c 's of 2.5, 1, and 0.5 MA/cm² for the irradiation doses of 0, 1, and 2×10^{14} He⁺/cm², respectively. It is apparent that no absolute correlation can be drawn between our measurements and either the critical current density or the resistive transition. The detection of nonlinearities below J_c in inductive measurements appears to be an independent measurement particularly sensitive to sample homogeneity.

V. CONCLUSIONS

A model explaining the response of a thin superconducting film to a nonuniform ac magnetic field has been developed. In developing the model, an expression was derived to predict the screening efficiency of thin films subjected to localized ac magnetic fields from small coils. In summary, the screening is proportional to the thickness of the film and even for films having thicknesses much less than the magnetic penetration depth, perfect

screening is an excellent approximation.

The model is successful in explaining the origin of third-harmonic components in the voltage generated across the coil. Full numerical solutions of this model yielded excellent agreement with the experiment data taken from high quality films. A simplified version of the model, with the film treated as a single annulus, enables the drive current corresponding to the critical current density to be rapidly estimated without having to measure the onset of a third-harmonic response. Once the third-harmonic onset drive current has been determined, the technique of Claassen, Reeves, and Soulen⁵ can be used to convert coil drive current to film current density. A more detailed calculation of the lateral current distribution without the assumption of perfect screening gave similar results.

The technique also provides a sensitive measure of the presence of weak links embedded in an epitaxial film. These weak links, which would be difficult to observe in a transport measurement, lead to excess harmonic generation at low drive currents in microcoil experiments. Ion irradiation at low energies with He⁺ ions was found to reduce the critical current density in our films without introducing weak-link behavior.

ACKNOWLEDGMENTS

The authors would like to thank David LeBlanc for his many hours spent winding our microcoils, Mark Reeves for some very useful comments regarding modeling of the experiment, and Ken Madden for several months of painstaking work before the apparatus was automated. We would like to express our appreciation for the financial support from both the Ontario Center for Materials Research (OCMR) and the Natural Sciences and Engineering Research Council of Canada (NSERC).

-
- ¹D. Dijkkamp, T. Venkatesan, X. D. Wu, S. A. Shaheen, N. Jisrawi, Y. H. Min-Lee, W. L. McLean, and M. Croft, *Appl. Phys. Lett.* **51**, 619 (1987).
²A. T. Fiory, A. F. Hebard, P. M. Mankiewich, and R. E. Howard, *Appl. Phys. Lett.* **52**, 2165 (1988); *Phys. Rev. Lett.* **61**, 1419 (1988).
³P. Scharnhorst, *Phys. Rev. B* **1**, 4295 (1970).
⁴K. Bernhardt *et al.*, *Physica C* **161**, 468 (1991).
⁵J. H. Claassen, M. E. Reeves, and R. J. Soulen, Jr., *Rev. Sci. Instrum.* **62**, 996 (1991).
⁶J. Z. Sun, M. J. Scharen, L. C. Bourne, and R. J. Schrieffer, *Phys. Rev. B* **44**, 5275 (1991).
⁷T. Ishida and R. B. Goldfarb, *Phys. Rev. B* **41**, 8937 (1990).
⁸C. Kittel, S. Fahey, and S. G. Louie, *Phys. Rev. B* **37**, 642 (1989).
⁹A more exact expression can be obtained as follows. Consider a filamentary current loop of radius r suspended a distance h above the film. The current density that results in the film can be shown to have a mean radius r . The width and magni-

tude of the current density scale as h and $1/h$, respectively, with a full width at half maximum of about $2h$. Since the equations are linear, the current distribution for a coil can be obtained by convolving these results over the coil dimensions. The result is that the effective width of the current distribution is given by $w = \{(\Delta r)^2 + (4h_0h_c + 2h_c^2)/\ln[(h_0 + h_c)/h_0]\}^{1/2}$, where h_c and h_0 are the height of the coil and the coil-to-film separation, and Δr is the width of the coil, i.e., the difference between the inner and outer radii. As the coil-to-film separation approaches zero, the current distribution width w approaches the coil width Δr .

- ¹⁰T. Van Duzer and C. W. Turner, *Principles of Superconductive Devices and Circuits* (Elsevier, North-Holland, Amsterdam, 1981), p. 115.
¹¹T. Ishida and H. Mazaki, *J. Appl. Phys.* **52**, 6798 (1981).
¹²T. Strach, M.S. thesis, McMaster University, 1992.
¹³F. W. Grover, *Inductance Calculations: Working Formulas and Tables* (Dover, New York, 1962).